









## Global projections of flash drought show increased risk in a warming climate

Jordan I. Christian <sup>1✉</sup>, Elinor R. Martin <sup>1</sup>, Jeffrey B. Basara <sup>1,2</sup>, Jason C. Furtado <sup>1</sup>, Jason A. Otkin <sup>3</sup>, Lauren E. L. Lowman <sup>4</sup>, Eric D. Hunt<sup>5</sup>, Vimal Mishra <sup>6,7</sup> & Xiangming Xiao <sup>8</sup>

Flash drought, characterized by unusually rapid drying, can have substantial impact on many socioeconomic sectors, particularly agriculture. However, potential changes to flash drought risk in a warming climate remain unknown. In this study, projected changes in flash drought frequency and cropland risk from flash drought are quantified using global climate model simulations. We find that flash drought occurrence is expected to increase globally among all scenarios, with the sharpest increases seen in scenarios with higher radiative forcing and greater fossil fuel usage. Flash drought risk over cropland is expected to increase globally, with the largest increases projected across North America (change in annual risk from 32% in 2015 to 49% in 2100) and Europe (32% to 53%) in the most extreme emissions scenario. Following low-end and medium scenarios compared to high-end scenarios indicates a notable reduction in annual flash drought risk over cropland.

<sup>1</sup>School of Meteorology, University of Oklahoma, Norman, OK, USA. <sup>2</sup>School of Civil Engineering and Environmental Science, University of Oklahoma, Norman, OK, USA. <sup>3</sup>Cooperative Institute for Meteorological Satellite Studies, Space Science and Engineering Center, University of Wisconsin-Madison, Madison, WI, USA. <sup>4</sup>Department of Engineering, Wake Forest University, Winston-Salem, NC, USA. <sup>5</sup>School of Natural Resources, University of Nebraska-Lincoln, Lincoln, NE, USA. <sup>6</sup>Civil Engineering, Indian Institute of Technology (IIT), Gandhinagar, India. <sup>7</sup>Earth Sciences, Indian Institute of Technology (IIT), Gandhinagar, India. <sup>8</sup>Department of Microbiology and Plant Biology, Center of Spatial Analysis, University of Oklahoma, Norman, OK, USA.  
✉email: [jchristian@ou.edu](mailto:jchristian@ou.edu)

According to the United Nations Population Division's medium scenario, global population is expected to increase to 9.7 billion in 2050 and 10.4 billion in 2100 from the projected global population of 8 billion at the end of 2022<sup>1</sup>. The associated demand for agriculture is expected to double by 2050, placing strain on sustainable and equitable food security globally<sup>2–4</sup>. Furthermore, projected increases in climate variability due to global climate change will impact the cropland expansion and agricultural intensification required to meet the demand in the coming decades<sup>5,6</sup>.

Of all weather and climate extremes, drought will likely bring the most complex challenges to food systems and agricultural productivity over the next century<sup>7–9</sup>. Drought of various types (e.g., meteorological, agricultural, hydrological) is projected to increase in frequency, severity, and spatial extent over many regions across the globe<sup>10–13</sup>. While changes in drought frequency across some locations are complicated due to uncertainties in precipitation<sup>10,14,15</sup> (e.g., the monsoon region in southeast Asia), elevated risk to drought is most consistently expected across Central America, Europe, and the Amazon<sup>10,11,16</sup>.

Flash drought presents a unique challenge within the realm of drought. Given their rapid development, drought mitigation strategies are challenging to implement during flash drought because these events often develop with limited warning, while leading to wide-ranging impacts across the land surface<sup>17</sup>. A notable example is the flash drought that occurred across western Russia during the summer of 2010. The event led to rapid land surface desiccation that promoted the development of a heatwave, resulting in high mortality and 11,000 excess deaths<sup>18</sup>. In addition, the flash drought conditions aided in wildfire development that resulted in severe air pollution and the displacement of thousands of people<sup>19,20</sup>. However, impacts from the flash drought were not limited to local scales. The timing of the 2010 flash drought occurred during a sensitive growing stage for winter and spring wheat crops and led to up to 70% lower wheat yields within top wheat producing oblasts in Russia<sup>21</sup>. As a result, the Russian government banned the export of wheat in August 2010, and wheat prices increased globally<sup>21,22</sup>.

Because of ever-growing demand for agricultural goods and increased risk to global food security over the twenty-first century, this study addresses two critical questions focused on flash drought: What are the projected trends in flash drought frequency across the globe in a warming climate, and how does agricultural risk from flash drought change in the future? These questions are addressed by identifying flash droughts using six models from the Coupled Model Intercomparison Project Phase 6 (CMIP6<sup>23</sup>). Historical simulations capture the period spanning 1850–2014, while three scenarios are used to project flash drought development under different socioeconomic pathways and radiative forcing levels for the years 2015–2100. The results identify flash drought characteristics in a warming climate and regions that are most susceptible to impacts from these events.

## Results

**Flash drought in the CMIP6 historical experiment.** To quantify flash drought development, evapotranspiration (ET), potential evapotranspiration (PET), and soil moisture were used from six CMIP6 models (Supplementary Table 1) on daily temporal scales for the historical, SSP126, SSP245, and SSP585 experiments. ET and PET were used to derive the standardized evaporative stress ratio<sup>24</sup> (SESR) and quantify the rate of intensification toward drought (the “flash” component of flash drought). Soil moisture was used to define moisture thresholds in flash drought development (the “drought” component of flash drought). SESR and soil moisture are sensitive to rapidly changing environmental

conditions toward flash drought<sup>18,24–28</sup>, provide early warning for drought development<sup>24,26,29</sup>, correspond with drought impacts indicated via the United States Drought Monitor<sup>24–26,30</sup> (USDM), and have been used to quantify flash drought development on spatial scales from local to global<sup>31–36</sup>.

We first examined the historical experiments from the CMIP6 models to determine how accurately the models captured the climatological characteristics of flash drought during the period spanning 1980–2014. Four reanalysis datasets (MERRA, MERRA-2, ERA Interim, and ERA5) were used to evaluate the performance of the CMIP6 models. CMIP6 flash drought frequency in most locations globally is within  $\pm 5\%$  of reanalysis-based flash drought occurrence for the period spanning 1980–2014, while only a few locations feature multi-model mean flash drought frequency significantly different ( $p < 0.1$ ) than the multi-reanalysis mean (e.g., the southeastern United States and eastern Europe; Supplementary Fig. 1). Overall, flash drought frequency is slightly underestimated in CMIP6 models at low to mid latitudes ( $0\text{--}40^\circ$ ) and slightly overestimated at high latitudes (poleward of  $40^\circ\text{N}$ ) in the Northern Hemisphere in comparison to the results from the reanalysis datasets.

In global hotspots of flash drought occurrence (i.e., 15 study regions selected with  $>30\%$  flash drought frequency between 1980 and 2014; Supplementary Fig. 2), the CMIP6 multi-model mean captures the seasonal cycle of flash drought occurrence depicted by reanalysis across a variety of climate types (Supplementary Fig. 3). Statistically significant agreement ( $p < 0.1$ ) exists in study regions with exceptions across the Iberian Peninsula, eastern Amazon, and the Indochinese Peninsula. Overall, with a few regional caveats, the historical comparison provides confidence that the composite of the CMIP6 models has skill representing flash drought development in future scenarios.

**Changes in flash drought frequency under future climate scenarios.** Toward the end of the twenty-first century (2066–2100), flash drought occurrence is projected to increase globally under all three future climate scenarios investigated (Fig. 1). The SSP126 scenario shows the smallest increase (6.0%), followed by SSP585 (8.2%), and then SSP245 (9.5%). Regionally, the largest projected increases in flash drought occurrence are in Europe and the Amazon. Dissimilar changes in flash drought frequency among the different scenarios are also evident over central Africa near the Sahel, India, and northern Australia. Flash drought occurrence is projected to remain unchanged or slightly increase over these regions for SSP126 and SSP245, but to decrease in SSP585.

Regional hotspots in flash drought occurrence (see Supplementary Fig. 2) reveal unique patterns in flash drought risk over time (Fig. 2). Between the mid-nineteenth century and early twenty-first century, 11 of the 15 study regions had a neutral trend over time (i.e.,  $<5\%$  change), with 7 regions having neither a statistically significant ( $p < 0.1$ ) increasing nor decreasing trend in flash drought (Supplementary Fig. 4). However, future projections of flash drought occurrence show increased frequency across most regions and SSP scenarios (12 of 15 regions in SSP126, 13 in SSP245, and 10 in SSP585), with statistically significant ( $p < 0.1$ ) increasing trends in flash drought over 6 of the study regions in SSP126, 10 in SSP245, and 7 in SSP585. Specifically, the SSP585 and SSP245 scenarios often show elevated flash drought frequency compared to SSP126 in regions where flash drought frequency increases through the twenty-first century (e.g., the Iberian Peninsula, eastern Europe, western Russia, eastern Amazon, and Asia Minor). In contrast, divergent trends exist across the various scenarios in northeastern China, India, the Great Rift Valley, and northern Australia. In these

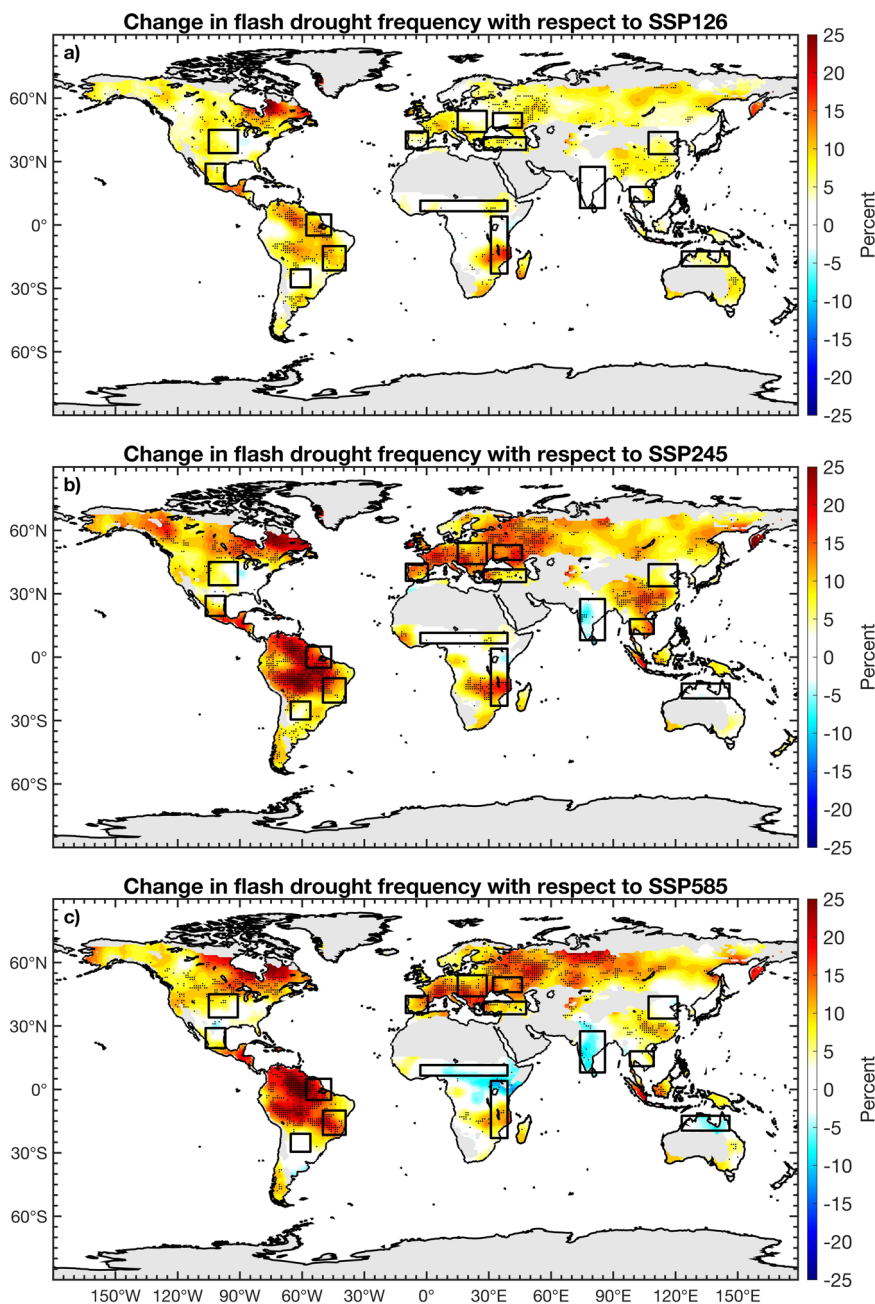


**Fig. 1 Impact of climate scenarios on flash drought frequency.** **a–c** The multi-model mean change in flash drought frequency between future climate change scenarios (2066–2100) and the historical period (1980–2014). The future climate change scenarios include **a** SSP126, **b** SSP245, and **c** SSP585. Unanimous agreement in the sign of the change among the models is stippled in black. Shaded regions in gray are masked areas that are either too arid or cold for flash drought development.

regions, SSP585 shows a decreasing trend in flash drought frequency, while SSP126 shows an increase in flash drought occurrence by the end of the twenty-first century. Further, flash drought frequency increases monotonically in the Sahel in the SSP126 and SSP245 scenarios, while the trend in the SSP585 scenario is decreasing in the early twenty-first century, before reversing in the mid-twenty-first century.

#### Cropland risk from flash drought under future scenarios.

Lower agricultural production is one of the primary impacts of flash drought<sup>21,29,37,38</sup>. As such, it is critical to understand how the risk to croplands from flash drought evolves under different climate scenarios. Globally, the models indicate that the

percentage of cropland area experiencing flash drought in the historical period (1850–2014) either decreased (Africa and Asia) or remained relatively stationary over time (Australia, North America, South America, and Europe; Fig. 3). In contrast, future projections show increases in cropland area affected by flash drought across all continents in all scenarios (Fig. 3). The largest increases between 2015 and 2100 (values taken from 30-year moving mean) are projected across North America (32–49%) and Europe (32–53%) in the SSP585 scenario, with notable increases also occurring across Africa (35–47%), Asia (28–38%), and South America (37–50%).

More complex changes in flash drought occurrence over croplands also exist, with SSP126 showing the highest risk to croplands over Australia and SSP245 projecting the lowest (and

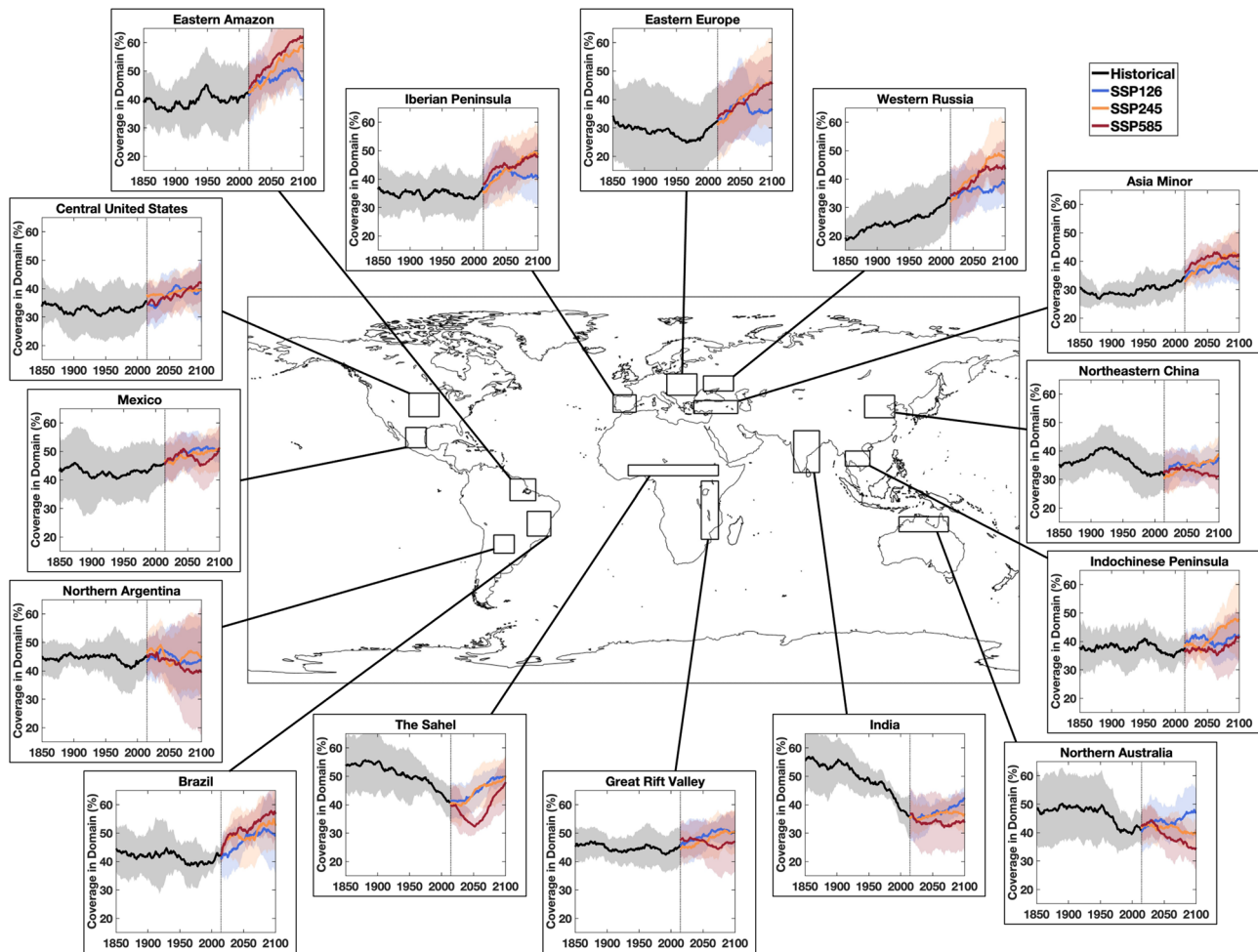


**Fig. 2** Yearly flash drought occurrence over hotspot regions. The multi-model mean yearly flash drought coverage in each study domain for historical (black), SSP126 (blue), SSP245 (orange), and SSP585 (red) models. A 30-year centered moving average is applied to each time series. The shaded regions indicate the variability ( $\pm 1\sigma$ ) among the 30-year centered moving averages between all six models for the corresponding historical and future scenarios.

minimal change to) cropland risk. Some continents also show evidence of a “tipping point” for flash drought risk (i.e., a large increase in flash drought risk to croplands between scenarios). Examples include Africa and North America, where the SSP126 and SSP245 scenarios generally project the same risk to croplands by 2100, but SSP585 shows a notable increase in flash drought risk to croplands.

## Discussion

Flash drought creates complex challenges for drought mitigation and early warning due to their rapid intensification of drought conditions. Because of rapid drought intensification, the lead time to impacts (e.g., agricultural yield loss, wildfires, heatwaves) is notably reduced compared to slower-developing conventional drought<sup>17</sup>. Increasing flash drought risk in a warming climate further amplifies the frequency of these impacts, and is particularly detrimental in areas where rapid agricultural yield loss can lead to the destabilization of regional economies<sup>21</sup>.

Given the limited knowledge of flash drought risk in a warming climate, this study highlights global projections of flash drought occurrence under different climate change scenarios in six CMIP6 models. In particular, this study quantifies trends in flash drought within global hotspot regions of flash drought occurrence, as well as changes in agricultural risk from flash drought. We illustrate a general increase in flash drought occurrence globally during the twenty-first century regardless of future scenario, with global flash

drought frequency increasing more with scenarios combining greater fossil fuel usage and higher radiative forcing (Fig. 1). Further, 11 of the 15 hotspot regions across the globe showed an increase in flash drought risk among all three climate projection scenarios between 2014 and 2100 (Fig. 2). Finally, all six continents are projected to experience an increased risk in flash drought over cropland among all scenarios (Fig. 3). Prior studies investigating flash drought projections in climate models in specific regions agree with our findings. For example, one study<sup>28</sup> showed an increasing risk of flash drought in the late twenty-first century over southeastern China, similar to that shown in Fig. 1. Further, another study<sup>39</sup> revealed that changes in flash drought frequency in a warming climate across India are complicated due to changes in the intraseasonal variability of monsoon precipitation (Fig. 1). Projections of flash drought characteristics have also shown that flash droughts are expected to increase in duration and severity (magnitude of drought)<sup>40</sup>.

Flash droughts develop due to the combination of precipitation deficits and enhanced evaporative demand<sup>41</sup>. How these two fundamental variables (precipitation and PET) evolve in a future climate can provide insight into the change of flash drought frequency associated with different climate change scenarios. Globally, annual mean precipitation amounts are expected to increase in many regions by the end of the twenty-first century (Supplementary Fig. 5). Flash drought hotspots with the largest precipitation increases have minimal changes in flash drought



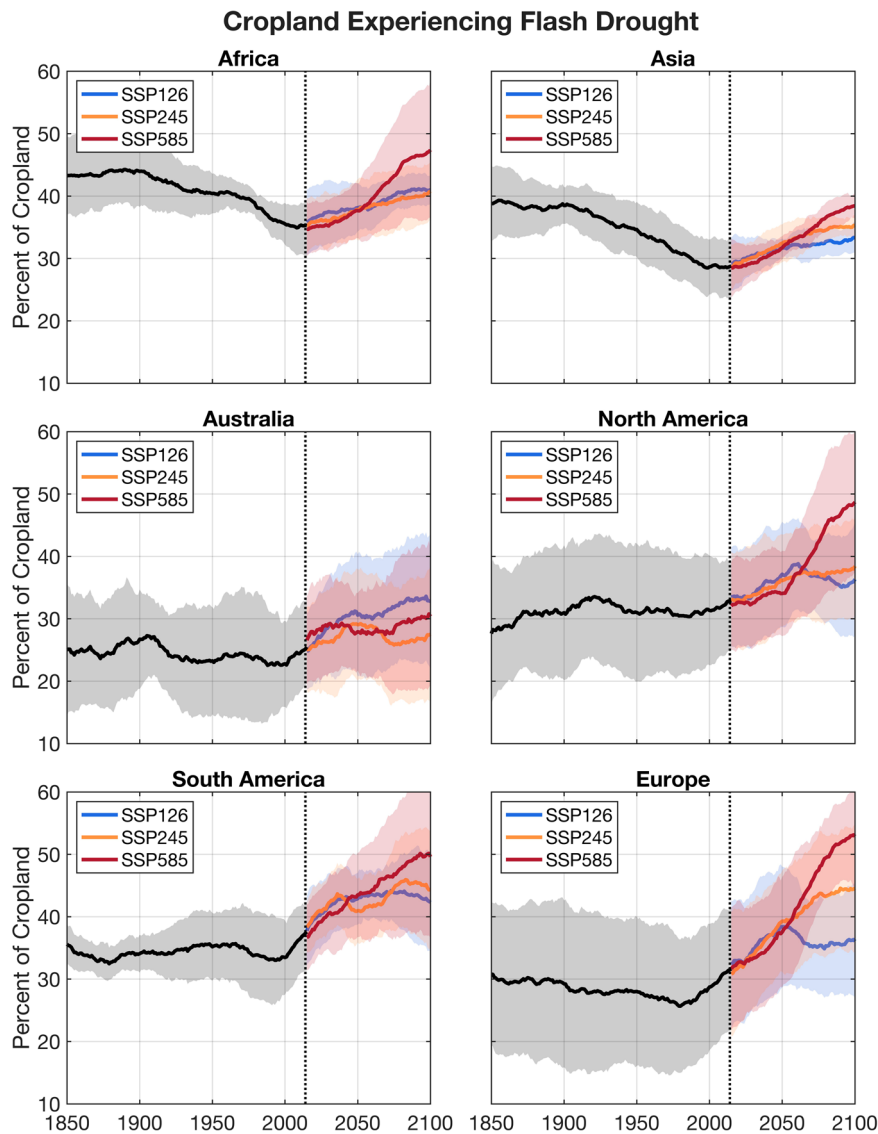


**Fig. 3 Flash drought risk over cropland.** The multi-model mean of the yearly percentage of cropland experiencing flash drought over entire continents for the historical (black), SSP126 (blue), SSP245 (orange), and SSP585 (red) scenarios. A 30-year centered moving average is applied to each time series. The shaded regions indicate the variability ( $\pm 1\sigma$ ) among the 30-year centered moving averages between all six models for the corresponding historical and future scenarios.

frequency (e.g., northeast China) or even a decrease in flash drought frequency (e.g., the Sahel and India, most evident in SSP585; Fig. 1 and Supplementary Fig. 5). However, some hotspots such as the Amazon, Iberian Peninsula, and Asia Minor, exhibit notable decreases in precipitation, especially in the SSP245 and SSP585 scenarios, and an associated increase in flash drought occurrence.

In addition to precipitation, increased PET can also contribute toward a higher frequency of flash drought. Even if precipitation remains relatively stationary over time across a region, consistently higher levels of evaporative demand will lead to a more rapid depletion of soil moisture and increase the likelihood of flash drought through increased ET. Temperature, a critical driver of evaporative demand<sup>42</sup>, will increase by the end of the twenty-first century globally, with larger changes linked to larger net radiative forcing (Supplementary Fig. 6). Temperatures are projected to increase more in higher latitudes (Supplementary Fig. 6). A similar pattern is seen for PET, with most regions equatorward of 30° experiencing relatively smaller increases in PET by the late twenty-first century (<5%, <10%, and <20% in SSP126, SSP245,

SSP585, respectively) compared to regions poleward of 30° with relatively large increases in evaporative demand (10–30%—SSP126, 15–40%—SSP245, 25–50%—SSP585; Supplementary Fig. 7). Overall, higher PET anomalies under future climate change scenarios overlap regions with expected increases in flash drought frequency (Fig. 1 and Supplementary Fig. 7). This relationship is most evident across Europe and in higher latitudes across North America, where a meridional gradient of increasing PET aligns with a gradient in increasing flash drought occurrence. Furthermore, regions with minimal increases in PET experience either a negligible change or a small decrease in flash drought frequency, compared to the historical period (e.g., the Sahel and India).

Among the primary drivers of flash drought (a lack of precipitation and increased evaporative demand), it is important to quantify their relative contributions to changes in flash drought frequency within future climate scenarios. Across the 14 hotspot regions where all three scenarios (SSP126, SSP245, and SSP585) show increasing flash drought frequency between the historical period (1980–2014) and the end of the twenty-first century

Change between Historical Period (1980–2014) and Future Projections (2066–2100)

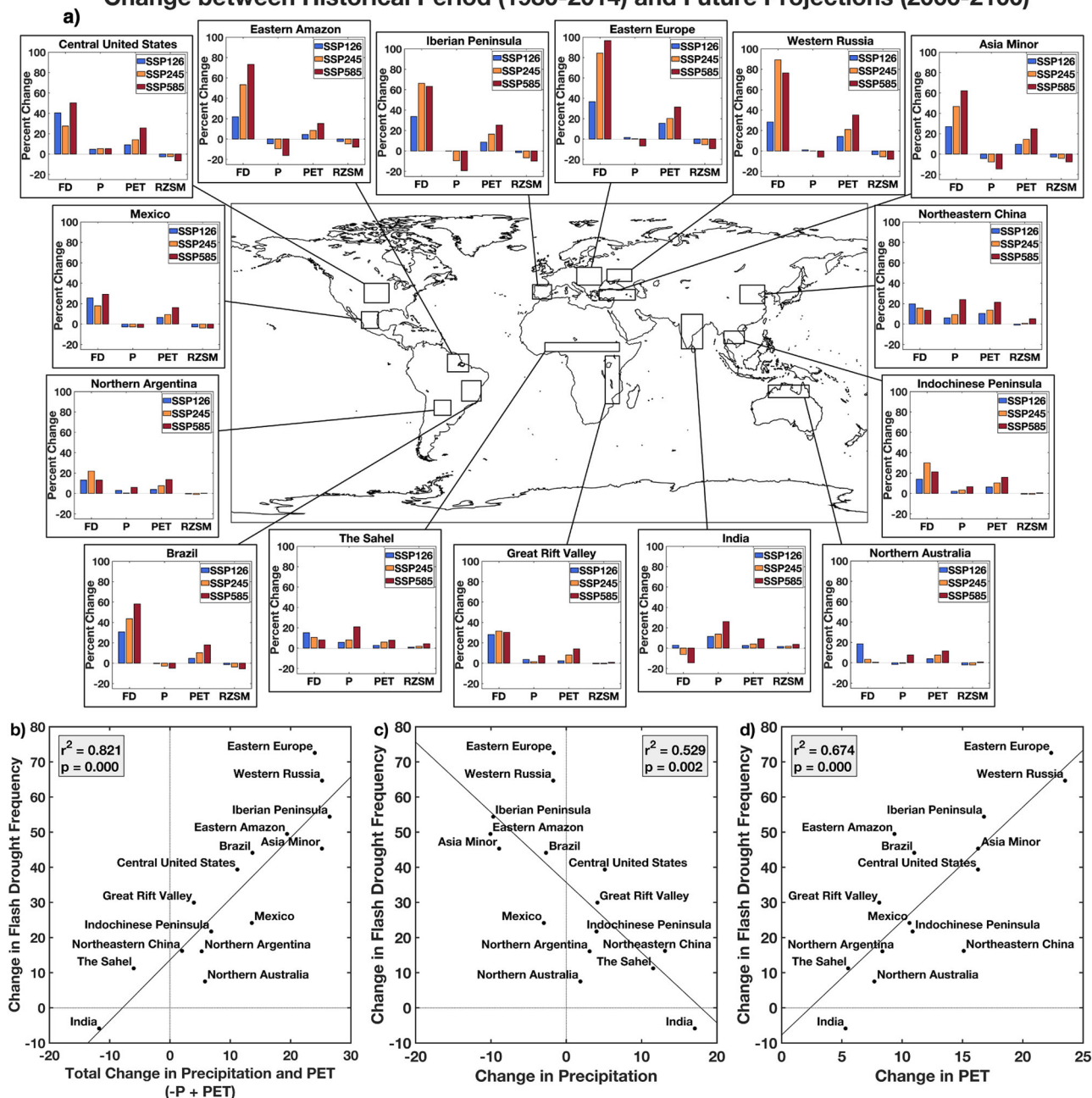


**Fig. 4 Drivers of flash drought over hotspot regions.** **a** The change in multi-model median between future scenarios (SSP126—blue, SSP245—orange, and SSP585—red for the years 2066–2100) and the historical period (1980–2014) for flash drought frequency (FD), precipitation (P), potential evapotranspiration (PET), and root zone soil moisture (RZSM) in each study domain. **b** Comparison of total change in precipitation and PET (-P + PET), **c** change in precipitation, and **d** change in potential evapotranspiration versus change in flash drought frequency between the mean of the future scenarios (2066–2100) and the historical period (1980–2014).

(2066–2100; all study regions except India), 13 regions are projected to have a larger positive percent change in PET than a negative change in precipitation, while 1 region exhibits a larger negative percent change in precipitation than a positive change in PET (eastern Amazon; Fig. 4). Within the context of historical models and reanalysis datasets during the development period of flash drought, precipitation has generally been found to be the primary driver of flash drought, while evaporative demand is an important secondary contributor<sup>31,43</sup>. However, within the context of climate change, increases in evaporative demand over the next century are projected to be larger, and as such, are likely more important to an increased risk in flash drought

development, compared to decreases in precipitation. While changes in soil moisture in the projections are minimal compared to changes in precipitation and evaporative demand, 9 of the 15 study regions have slight drying (mean of scenarios between -0.2 and -6.5%) in soil moisture by the end of the twenty-first century (Fig. 4). The coefficient of determination also indicates that the explained variance in changes of flash drought frequency from changes in PET (67.4%) is higher than the explained variance in changes of flash drought frequency from changes in precipitation (52.9%; Fig. 4). However, it is important to note that the strongest relationship and highest explained variance of changes in flash drought frequency is with the combined, total

change in precipitation and PET (Fig. 4), reinforcing the critical point that the risk of flash drought is greatest with the combination of reduced precipitation and increased PET<sup>24,41</sup>.

A critical aspect of flash drought is the rate of drought intensification. This defining characteristic of flash drought (compared to slower, conventional drought development) drastically reduces the development time toward wide-ranging impacts including agricultural losses, ecosystem stress, wildfire development, and reduction in water resources<sup>37,41,44,45</sup>. These impacts may be further exacerbated in the future if intensification rates of flash drought increase over time. Across all climate change scenarios, flash drought intensification rate is expected to increase globally, with the largest increases seen in SSP585 (32.1%; Supplementary Fig. 8) and specifically in northern South America, the Sahel, and parts of India (>70%).

Several factors promote faster drought intensification, such as higher levels of evaporative demand and differences in land cover type<sup>18,44,46,47</sup>. Globally, PET is projected to increase through the twenty-first century, and likely is the most important driver in the overall global increase in flash drought intensification rates (Supplementary Figs. 7 and 8). However, local variations in intensification rates are due to other factors. For example, the global maxima in intensification rate across northern South America, particularly the Amazon region, are also spatially aligned with large decreases in primary forest cover (Supplementary Fig. 9). Conversion of forested lands in the Amazon from forests to croplands and pastures alters the climate by extending dry periods<sup>48,49</sup>. Deforestation leads to decreases in ET, as less vegetation is present to undergo photosynthesis, and decreases in rainfall over deforested regions, as changes in the energy and water budgets create dryer conditions overall<sup>50,51</sup>. Because forests are more resilient to flash drought development compared to grasslands and agricultural lands<sup>18,44,47</sup>, accelerated deforestation in more aggressive socioeconomic pathways exacerbates the increase in flash drought intensification rate.

Under future climate change, not only will croplands be at greater risk for drought<sup>52</sup> but croplands will also be more susceptible to a higher frequency of flash drought (Fig. 3). In the twenty-first century, considerable cropland expansion and intensification is expected regardless of the socioeconomic pathway, especially in Africa and South America (Supplementary Fig. 10). As such, the total cropland area projected to experience flash drought also rises throughout the future period. However, the relative percentage of agricultural land that is impacted by rapid drought intensification also increases due to the projections of higher frequency in flash drought occurrence (Figs. 2 and 3). Because of this, even as cropland expansion continues in the coming decades to account for the increasing demand in agriculture, challenges in meeting global food demand will be further exacerbated by the increasing risk of cropland to flash drought development.

The projections of agricultural risk also highlight the importance of even so-called moderate scenarios (such as SSP245) compared to more aggressive scenarios (i.e., SSP585) of future climate change. Under the SSP585 scenario, all continents except for Australia experience the largest increase in agricultural risk to flash drought compared to SSP126 and SSP245 scenarios (Fig. 3). However, North America, Africa, and to some extent, South America show a dramatic rise in cropland experiencing flash drought on an annual basis if the SSP585 scenario is followed, while SSP126 and SSP245 remain relatively similar and flash drought risk is notably reduced.

As global population increases and the demand for agriculture grows, changes in the frequency of flash drought will further strain food security in the future. Indeed, flash drought creates additional challenges by reducing the access to our fundamental needs for food and water on timescales much faster than slower-developing, conventional drought. This study reveals agricultural

regions across the globe that may be most susceptible to more frequent and intense flash droughts in a changing climate and therefore have the greatest exposure to flash drought impacts to agricultural production. Moving forward, future research is needed to explore the region-dependent atmospheric and oceanic drivers of flash drought development in a future climate (teleconnections, upper-level atmospheric wave patterns, etc.). Further, local-scale impacts and mitigation strategies for flash drought necessitate additional investigation based on the projected changes in flash drought occurrence within the context of global warming.

## Methods

**Data.** Land-use data is taken from the Land-Use Harmonization (LUH2 v2f) project<sup>53</sup>. LUH2 provides land-use states for the historical (1850–2014) and future (2015–2100) period in the CMIP6 models on annual scales with a spatial resolution of 0.25°. The historical and future SSP land-use scenarios<sup>54</sup> (SSP126, SSP245, and SSP585) were used for analysis in conjunction with the corresponding CMIP6 experiments. It is important to note that while CMIP6 models use the same land use and land cover (LULC) dataset (LUH2 v2f), uncertainty in classifying different LULC categories may exist. These uncertainties can impact CO<sub>2</sub> emissions and the global carbon cycle<sup>55</sup>, and earth system models can be sensitive to changes in LULC<sup>56,57</sup>. Certain LULC types may be more susceptible or resilient to flash drought development (e.g., forests vs. grasslands vs. cropland)<sup>18,44</sup>. However, most areas globally are projected to have increases in flash drought occurrence over a wide range of LULC types (Fig. 1). As such, any uncertainties in LULC within future projections may impact the magnitude of changes in flash drought frequency, but the overall trend in flash drought occurrence will remain the same.

Historical flash drought was quantified using four global reanalysis datasets: MERRA<sup>58</sup>, MERRA-2<sup>59</sup>, ERA-Interim<sup>60</sup>, and ERA5<sup>61</sup>. Several studies have shown that these reanalysis datasets are able to effectively capture flash drought from a climatological perspective and case study analysis<sup>18,24,25,31,33,46,62–64</sup>. CMIP6 models<sup>33</sup> were used in this study for the historical modeling and future projection of flash drought, with details of each model provided in Supplementary Table 1. Models were selected from the CMIP6 experiment based on the availability of variables necessary for flash drought analysis (ET, PET, and soil moisture) on daily time scales and scenarios used in the analysis (historical, SSP126, SSP245, SSP585). Given these requirements, six models provided the necessary data for this study (IPSL-CM6A-LR, MPI-ESM1-2-HR, MPI-ESM1-2-LR, MRI-ESM2-0, NorESM2-LM, and NorESM2-MM; Supplementary Table 1).

Daily ET, PET, and near-surface soil moisture were obtained from the four global reanalysis datasets between 1980–2014, between 1850 and 2014 for the historical models, and between 2015 and 2100 for the future scenarios. Daily PET was derived from each dataset using the Food and Agriculture Organization Penman–Monteith equation<sup>65</sup>. It is important to note that PET calculated via the Penman–Monteith equation (and other common PET formulations) does not consider the role of increased CO<sub>2</sub> concentration in warming climate and may lead to overestimation of drying in variables that incorporate PET<sup>66</sup>. Despite this limitation, this study focuses on flash drought and the rate of drought intensification, and not the overall magnitude of drying. In the CMIP6 models, wind speed is provided at 10 m. However, 2-m wind speed was approximated from 10-meter wind speed using the method in ref. <sup>67</sup> to incorporate into the equation for PET. Daily values of the evaporative stress ratio (ESR) were calculated by taking the ratio between daily ET and PET. Mean pentad values of ESR and soil moisture were computed and ESR was standardized at each grid point to calculate the standardized ESR (SESR). SESR is given as:

$$\text{SESR}_{ijp} = \frac{\text{ESR}_{ijp} - \overline{\text{ESR}}_{ijp}}{\sigma_{\text{ESR}_{ijp}}}$$

where  $\text{SESR}_{ijp}$  (referred to as SESR) is the  $z$  score of ESR at a specific grid point ( $i, j$ ) for a specific pentad  $p$ ,  $\overline{\text{ESR}}$  is the mean ESR at a specific grid point ( $i, j$ ) for a specific pentad  $p$  for the years between 1980 and 2014, and  $\sigma_{\text{ESR}}$  is the standard deviation of ESR at a specific grid point ( $i, j$ ) for a specific pentad  $p$  for the years between 1980 and 2014.

To account for pentad-to-pentad variability in SESR, the Savitzky–Golay filter<sup>68</sup> was used to smooth the time series of SESR at each grid point while preserving higher moments in the data<sup>32</sup>. Following guidance from applications to remote sensing observations<sup>69</sup>,  $d = 4$  was used for the degree of polynomial, and  $m = 10$  was used as the half-width of the smoothing window (full window length of 21 pentads). The Savitzky–Golay filter with the same degree of polynomial and window length was also applied to soil moisture at each grid point.

Following the calculation of SESR and the Savitzky–Golay filter, the temporal change in SESR was calculated and standardized as:

$$\left(\Delta\text{SESR}_{ijp}\right)_z = \frac{\Delta\text{SESR}_{ijp} - \overline{\Delta\text{SESR}}_{ijp}}{\sigma_{\Delta\text{SESR}_{ijp}}}$$



where  $(\Delta\text{SESR}_{ijp})_z$  (referred to as  $\Delta\text{SESR}$ ) is the  $z$ -score of the change in SESR from one pentad to another pentad at a specific grid point  $(i, j)$  for a specific pentad  $p$ ,  $\Delta\text{SESR}$  is the mean change in SESR values at a specific grid point  $(i, j)$  for a specific pentad  $p$  for the years between 1980–2014, and  $\sigma_{\Delta\text{SESR}}$  is the standard deviation of SESR changes at a specific grid point  $(i, j)$  for a specific pentad  $p$  for the years between 1980 and 2014.

**Flash drought identification.** Flash drought is characterized by the rapid intensification of drought conditions<sup>24,41</sup>. In this study, flash drought events were identified using a modified framework from a previously established identification methodology<sup>24</sup>. The methodology used in this study uses three criteria, with two focusing on the impacts of drought and one emphasizing the rapid drought intensification<sup>32</sup>. These criteria are:

1.  $\Delta\text{SESR}$  must be at or below the 25th percentile of  $\Delta\text{SESR}$  values.
2. A minimum length of five pentad changes in SESR, equivalent to a length of six pentads (30 days).
3. A final soil moisture value below the 20th percentile of soil moisture values.

Percentiles for criterion 1 were taken from the distribution of  $\Delta\text{SESR}$  and percentiles for criterion 3 were taken from the distribution of soil moisture at each grid point and specific pentads for the years between 1980–2014 in the dataset. Percentiles were drawn from the distribution of  $\Delta\text{SESR}$  and soil moisture between 1980–2014 in order to have the same temporal window of analysis between the reanalysis datasets and historical models and to maintain a consistent reference frame for the entire length of the climate models (1850–2100). Criteria 2 and 3 are used to capture land-surface impacts associated with flash drought development. The second criterion is used to delineate between short-term dry spells and events where rapid drought intensification leads to drought impact. The 20th percentile threshold associated with the third criterion satisfies the drought component of flash drought<sup>41</sup>.

Flash droughts were identified between March through October in Northern Hemisphere latitudes greater than 30°N and between September through April in Southern Hemisphere latitudes poleward of 30°S. This is due to limitations on evaporative demand during the cool season such that rapid drought intensification is highly constrained<sup>24</sup>. Flash droughts were identified throughout the year in equatorial latitudes (between 30°S and 30°N) as high levels of evaporative demand are available year-round.

In previous studies using the original SESR flash drought methodology<sup>18,24,25,27,31,62,63,70–74</sup>, two separate but complementary criteria were used to identify the rapid rate of intensification toward drought (i.e., the “flash” component of flash drought). The two criteria were used to account for pentad-to-pentad variability in the rate of drought intensification during flash drought. However, the application of the Savitzky-Golay filter on the SESR time series allows for a simplification of these criteria, such that an individual criterion ( $\Delta\text{SESR}$  less than or equal to the 25th percentile) can be used to identify rapid drought intensification<sup>32</sup>.

In addition, soil moisture was used to determine if drought conditions were reached during the flash drought event. In the original SESR flash drought framework, SESR values below the 20th percentile were used to verify that drought conditions were achieved during flash drought<sup>24</sup>. However, given the multi-century timescales examined in this study and the complex changes of SESR over large time periods due to changes in temperature, precipitation, vapor pressure deficit, and several other thermal, moisture, and radiative flux variables, soil moisture was used in place of SESR in criterion 3.

Reliable and robust results for climate projections of flash drought may be particularly challenging, given that flash drought event identification is sensitive to the datasets, variables, and identification methodology used in the analysis<sup>27,63</sup>. This study leveraged several approaches to increase reliability and robustness of the results presented here. First, this study utilizes a multi-dataset, multi-model, ensemble approach to flash drought identification. Thus, while results from an individual dataset may vary from other datasets, more robust signals can be captured from the mean of multiple datasets<sup>31,43</sup>. In this study, six CMIP6 models were used to contribute to the multi-model mean, and the climatological characteristics of flash drought from the historical model mean were found to be similar to the mean results from four reanalysis datasets (Supplementary Figs. 1 and 3).

Second, a multi-variate approach for flash drought identification<sup>17,32,63</sup> was used to increase the robustness of the results and to minimize variability created by using single variable approaches to flash drought detection. ET-based metrics and soil moisture are the two most commonly used indicators to define flash drought<sup>75</sup> and while most studies use one of these metrics to identify flash drought, this study combines the utility of evaporative stress and soil moisture to identify the “flash” component (via evaporative stress) and the “drought” component (via soil moisture) of rapid drought intensification. Further, evaporative stress is multivariate in and of itself, as it represents the ratio between available moisture at the land surface and the atmospheric demand<sup>24,76–78</sup>.

Finally, flash drought identification should identify previously known and notable flash drought events and correspond with drought impacts indicated by other drought metrics. This study utilized a modified version of the Christian et al. (2019, 2022)<sup>24,32</sup> identification approach which, in conjunction with SESR, has captured the spatial and temporal evolution of major flash droughts events (e.g., central United States in 2012 and southwestern Russia in 2010)<sup>18,25</sup>, compares

favorably with the United States Drought Monitor<sup>24,25</sup> (USDM), and corresponds to land surface desiccation detected via satellite remote sensing<sup>18,24,32</sup>. An example of the major flash drought event across the central United States in 2012<sup>25,29,44</sup> using the identification framework in this study is shown in Supplementary Fig. 11.

**Ensemble averaging.** Flash drought events were identified in each reanalysis dataset and model. A particular year was labeled a “flash drought year” if at least one flash drought occurred. Subsequently, datasets were averaged for each segment of the analysis, such that historical observations via the four reanalysis datasets were averaged together, the six historical CMIP6 models were averaged together, and future projections from the six CMIP6 models were averaged for each scenario (SSP126, SSP245, and SSP585). Because the reanalysis and CMIP6 datasets have different spatial resolutions, composited spatial maps were produced by (1) bilinearly interpolating each dataset to a new grid with a spatial resolution of  $0.5^\circ \times 0.5^\circ$ , and (2) and calculating the mean between the newly interpolated gridded datasets.

For time series, all grid points that underwent flash drought for a given year were accumulated and were then converted to a percentage, representing flash drought spatial coverage with respect to the entire domain. This yearly percentage was then averaged between the appropriate datasets to produce each time series.

Grid points for locations that are too arid or cold were masked on each spatial map. Arid locations were determined by calculating the aridity index as:

$$\text{AI} = \frac{P}{\text{PET}}$$

where  $P$  is the average annual precipitation and PET is the average annual potential ET from the MERRA-2 dataset between the years 1980 and 2014. Specifically, grid points were masked where the average annual aridity index was below 0.2 (arid and hyper-arid locations) or where the average daily PET was  $<1$  mm/day during the growing season for the Northern Hemisphere (March through October) and Southern Hemisphere (September through April). The aridity threshold was used to place an emphasis on rapid drought development in regions that can transition from more humid to drier environmental conditions and are more likely to experience vegetative, agricultural, or environmental effects from flash drought. In addition, the PET threshold requires regions to have enough evaporative demand throughout the growing season to allow for higher ET rates, sufficient soil moisture depletion, and increased evaporative stress to create rapid drought development.

In this study, an ensemble averaging approach with the CMIP6 models was used instead of individual bias correction of each model. Bias correction methods may improve climatological means for a specific variable, but can also generate additional biases, such as an increased bias in variability<sup>79</sup>. Further, bias correction techniques are unable to correct future climate trends<sup>80,81</sup> and can also lead to unphysical trends in future projections<sup>82</sup>. Because of these limitations, spatial and temporal comparisons of multi-model means between the CMIP6 models and reanalysis datasets were analyzed (Supplementary Figs. 1 and 3). Overall, it was found that the ensemble averaging approach for the CMIP6 models was able to represent flash drought characteristics compared to the mean of the reanalysis datasets for most regions across the globe (Supplementary Figs. 1 and 3).

## Data availability

Variables and derived variables used in this study from MERRA and MERRA-2 are available at <https://disc.gsfc.nasa.gov>, from ERA-Interim are available at <https://apps.ecmwf.int/datasets/>, and from ERA5 are available at <https://cds.climate.copernicus.eu>. CMIP6 data are available at <https://esgf-node.llnl.gov/projects/cmip6/>.

## Code availability

The code used for this study is available at <https://doi.org/10.5281/zenodo.7796371>.

Received: 10 November 2022; Accepted: 26 April 2023;

Published online: 25 May 2023

## References

1. United Nations. *World Population Prospects 2022: Summary of Results*. UN DESA/POP/2022/TR/NO. 3 (UN, 2022).
2. Godfray, H. C. J. et al. Food security: the challenge of feeding 9 billion people. *Science* **327**, 812–818 (2010).
3. Spiertz, J. H. J. & Ewert, F. Crop production and resource use to meet the growing demand for food, feed and fuel: opportunities and constraints. *NJAS - Wageningen J. Life Sci.* **56**, 281–300 (2009).
4. Tilman, D., Balzer, C., Hill, J. & Befort, B. L. Global food demand and the sustainable intensification of agriculture. *Proc. Natl Acad. Sci. USA* **108**, 20260–20264 (2011).



5. Seager, R., Naik, N. & Vogel, L. Does global warming cause intensified interannual hydroclimate variability? *J. Clim.* **25**, 3355–3372 (2012).
6. Thornton, P. K., Ericksen, P. J., Herrero, M. & Challinor, A. J. Climate variability and vulnerability to climate change: a review. *Glob. Chang. Biol.* **20**, 3313–3328 (2014).
7. Cheeseman, J. in *Halophytes for Food Security in Dry Lands* (eds Khan, M. A., Ozturk, M., Gul, B. & Ahmed, M. Z.) 111–123 (Academic, 2016)
8. Gregory, P. J., Ingram, J. S. I. & Brklacich, M. Climate change and food security. *Philos. Trans. R. Soc. B Biol. Sci.* **360**, 2139–2148 (2005).
9. Ziervogel, G. & Ericksen, P. J. Adapting to climate change to sustain food security. *Wiley Interdiscip. Rev. Clim. Chang.* **1**, 525–540 (2010).
10. Cook, B. I. et al. Twenty-first century drought projections in the CMIP6 forcing scenarios. *Earth's Future* **8**, e2019EF001461 (2020).
11. Lu, J., Carbone, G. J. & Grego, J. M. Uncertainty and hotspots in 21st century projections of agricultural drought from CMIP5 models. *Sci. Rep.* **9**, 4922 (2019).
12. Wang, T., Tu, X., Singh, V. P., Chen, X. & Lin, K. Global data assessment and analysis of drought characteristics based on CMIP6. *J. Hydrol.* **596**, 126091 (2021).
13. Ukkola, A. M., Kauwe, M. G. D., Roderick, M. L., Abramowitz, G. & Pitman, A. J. Robust future changes in meteorological drought in cmip6 projections despite uncertainty in precipitation. *Geophys. Res. Lett.* **47**, e2020GL087820 (2020).
14. Aadhar, S. & Mishra, V. On the projected decline in droughts over South Asia in CMIP6 multimodel ensemble. *J. Geophys. Res. Atmos.* **125**, e2020JD033587 (2020).
15. Wang, B., Jin, C. & Liu, J. Understanding future change of global monsoons projected by CMIP6 models. *J. Clim.* **33**, 6471–6489 (2020).
16. Zhao, T. & Dai, A. CMIP6 model-projected hydroclimatic and drought changes and their causes in the 21st century. *J. Clim.* <https://doi.org/10.1175/jcli-d-21-0442.1> (2021).
17. Otkin, J. A. et al. Getting ahead of flash drought: from early warning to early action. *Bull. Am. Meteorol. Soc.* <https://doi.org/10.1175/bams-d-21-0288.1> (2022)
18. Christian, J. I., Basara, J. B., Hunt, E. D., Otkin, J. A. & Xiao, X. Flash drought development and cascading impacts associated with the 2010 Russian heatwave. *Environ. Res. Lett.* **15**, 094078 (2020).
19. Bondur, V. G. Satellite monitoring of wildfires during the anomalous heat wave of 2010 in Russia. *Izvestiya Atmos. Ocean Phys.* **47**, 1039–1048 (2011).
20. Shaposhnikov, D. et al. Mortality related to air pollution with the Moscow heat wave and wildfire of 2010. *Epidemiology* **25**, 359–364 (2014).
21. Hunt, E. et al. Agricultural and food security impacts from the 2010 Russia flash drought. *Weather Clim. Extremes* **34**, 100383 (2021).
22. Welton, G. The impact of Russia's 2010 grain export ban. *Oxfam Research Report* 1–32 (Oxfam, 2011).
23. Eyring, V. et al. Overview of the coupled model intercomparison project phase 6 (CMIP6) experimental design and organization. *Geosci. Model Dev.* **9**, 1937–1958 (2016).
24. Christian, J. I. et al. A methodology for flash drought identification: application of flash drought frequency across the United States. *J. Hydrometeorol.* **20**, 833–846 (2019).
25. Basara, J. B. et al. The evolution, propagation, and spread of flash drought in the Central United States during 2012. *Environ. Res. Lett.* **14**, 084025 (2019).
26. Ford, T. W., McRoberts, D. B., Quiring, S. M. & Hall, R. E. On the utility of in situ soil moisture observations for flash drought early warning in Oklahoma, USA. *Geophys. Res. Lett.* **42**, 9790–9798 (2015).
27. Osman, M. et al. Flash drought onset over the contiguous United States: sensitivity of inventories and trends to quantitative definitions. *Hydrol. Earth Syst. Sci.* **25**, 565–581 (2021).
28. Yuan, X. et al. Anthropogenic shift towards higher risk of flash drought over China. *Nat. Commun.* **10**, 4661 (2019).
29. Otkin, J. A. et al. Assessing the evolution of soil moisture and vegetation conditions during the 2012 United States flash drought. *Agric. Forest Meteorol.* **218**, 230–242 (2016).
30. Otkin, J. A. et al. Development of a flash drought intensity index. *Atmosphere* **12**, 741 (2021).
31. Christian, J. I. et al. Global distribution, trends, and drivers of flash drought occurrence. *Nat. Commun.* **12**, 6330 (2021).
32. Christian, J. I. et al. Flash drought identification from satellite-based land surface water index. *Remote Sens. Appl. Soc. Environ.* **26**, 100770 (2022).
33. Koster, R. D., Schubert, S. D., Wang, H., Mahanama, S. P. & DeAngelis, A. M. Flash drought as captured by reanalysis data: disentangling the contributions of precipitation deficit and excess evapotranspiration flash drought as captured by reanalysis data: disentangling the contributions of precipitation deficit and excess evapotranspiration. *J. Hydrometeorol.* **20**, 1241–1258 (2019).
34. Mukherjee, S. & Mishra, A. K. A multivariate flash drought indicator for identifying global hotspots and associated climate controls. *Geophys. Res. Lett.* **49**, e2021GL096804 (2022).
35. Otkin, J. A. et al. Assessing the evolution of soil moisture and vegetation conditions during a flash drought–flash recovery sequence over the South-Central United States. *J. Hydrometeorol.* **20**, 549–562 (2019).
36. Sehgal, V., Gaur, N. & Mohanty, B. P. Global flash drought monitoring using surface soil moisture. *Water Resour. Res.* **57**, e2021WR029901 (2021).
37. Hoell, A. et al. Lessons learned from the 2017 flash drought across the U.S. Northern Great Plains and Canadian Prairies. *Bull. Am. Meteorol. Soc.* **101**, E2171–E2185 (2020).
38. Otkin, J. A., Haigh, T., Mucia, A., Anderson, M. C. & Hain, C. Comparison of agricultural stakeholder survey results and drought monitoring datasets during the 2016 U.S. Northern Plains flash drought. *Weather Clim. Soc.* **10**, 867–883 (2018).
39. Mishra, V., Aadhar, S. & Mahto, S. S. Anthropogenic warming and intraseasonal summer monsoon variability amplify the risk of future flash droughts in India. *Npj Clim. Atmos. Sci.* **4**, 1 (2021).
40. Sreeparvathy, V. & Srinivas, V. V. Meteorological flash droughts risk projections based on CMIP6 climate change scenarios. *Npj Clim. Atmos. Sci.* **5**, 77 (2022).
41. Otkin, J. A. et al. Flash droughts: a review and assessment of the challenges imposed by rapid onset droughts in the United States. *Bull. Am. Meteorol. Soc.* **99**, 911–919 (2018).
42. Hobbins, M., Wood, A., Streubel, D. & Werner, K. What drives the variability of evaporative demand across the conterminous United States? *J. Hydrometeorol.* **13**, 1195–1214 (2012).
43. Hoffmann, D., Gallant, A. J. E. & Hobbins, M. Flash drought in CMIP5 models. *J. Hydrometeorol.* <https://doi.org/10.1175/jhm-d-20-0262.1> (2021)
44. Jin, C. et al. The 2012 flash drought threatened US midwest agroecosystems. *Chin. Geogr. Sci.* **29**, 768–783 (2019).
45. Zhang, M., Yuan, X. & Otkin, J. A. Remote sensing of the impact of flash drought events on terrestrial carbon dynamics over China. *Carbon Balance Manag.* **15**, 20 (2020).
46. Chen, L., Ford, T. W. & Yadav, P. The role of vegetation in flash drought occurrence: a sensitivity study using community earth system model, version 2. *J. Hydrometeorol.* **22**, 845–857 (2021).
47. Zhang, M. & Yuan, X. Rapid reduction in ecosystem productivity caused by flash droughts based on decade-long FLUXNET observations. *Hydrol. Earth Syst. Sci.* **24**, 5579–5593 (2020).
48. Malhi, Y. et al. Exploring the likelihood and mechanism of a climate-change-induced dieback of the Amazon rainforest. *Proc. Natl Acad. Sci. USA* **106**, 20610–20615 (2009).
49. Butt, N., Oliveira, P. A. de & Costa, M. H. Evidence that deforestation affects the onset of the rainy season in Rondonia, Brazil. *J. Geophys. Res. Atmos.* <https://doi.org/10.1029/2010JD015174> (2011).
50. Coe, M. T., Costa, M. H. & Soares-Filho, B. S. The influence of historical and potential future deforestation on the stream flow of the Amazon River – Land surface processes and atmospheric feedbacks. *J. Hydrol.* **369**, 165–174 (2009).
51. Davidson, E. A. et al. The Amazon basin in transition. *Nature* **481**, 321–328 (2012).
52. Li, Y., Ye, W., Wang, M. & Yan, X. Climate change and drought: a risk assessment of crop-yield impacts. *Clim. Res.* **39**, 31–46 (2009).
53. Hurtt, G. C. et al. Harmonization of global land use change and management for the period 850–2100 (LUH2) for CMIP6. *Geosci. Model Dev.* **13**, 5425–5464 (2020).
54. Popp, A. et al. Land-use futures in the shared socio-economic pathways. *Glob. Environ. Chang.* **42**, 331–345 (2017).
55. Lawrence, P. J., Lawrence, D. M. & Hurtt, G. C. Attributing the carbon cycle impacts of CMIP5 historical and future land use and land cover change in the community earth system model (CESM1). *J. Geophys. Res. Biogeosci.* **123**, 1732–1755 (2018).
56. Malyshev, S., Shevliakova, E., Stouffer, R. J. & Pacala, S. W. Contrasting local versus regional effects of land-use-change-induced heterogeneity on historical climate: analysis with the GFDL earth system model. *J. Clim.* **28**, 5448–5469 (2015).
57. Ma, L. et al. Global rules for translating land-use change (LUH2) to land-cover change for CMIP6 using GLM2. *Geosci. Model Dev.* **13**, 3203–3220 (2020).
58. Rienecker, M. M. et al. MERRA: NASA's modern-era retrospective analysis for research and applications. *J. Clim.* **24**, 3624–3648 (2011).
59. Gelaro, R. et al. The modern-era retrospective analysis for research and applications, version 2 (MERRA-2). *J. Clim.* **30**, 5419–5454 (2017).
60. Dee, D. P. et al. The ERA-Interim reanalysis: configuration and performance of the data assimilation system. *Q. J. R. Meteorol. Soc.* **137**, 553–597 (2011).
61. Hersbach, H. et al. The ERA5 global reanalysis. *Q. J. R. Meteorol. Soc.* **146**, 1999–2049 (2020).
62. Christian, J. I., Basara, J. B., Otkin, J. A. & Hunt, E. D. Regional characteristics of flash droughts across the United States. *Environ. Res. Commun.* **1**, 125004 (2019).
63. Mukherjee, S. & Mishra, A. K. Global flash drought analysis: uncertainties from indicators and datasets. *Earth's Future* **10**, e2022EF002660 (2022).

64. Parker, T., Gallant, A., Hobbins, M. & Hoffmann, D. Flash drought in Australia and its relationship to evaporative demand. *Environ. Res. Lett.* **16**, 064033 (2021).
65. Allen, R. G., Pereira, L. S., Raes, D. & Smith, M. *Crop Evapotranspiration-Guidelines For Computing Crop Water Requirements*. FAO Irrigation and Drainage Paper 56 (FAO, 1998).
66. Milly, P. C. D. & Dunne, K. A. Potential evapotranspiration and continental drying. *Nat. Clim. Chang.* **6**, 946–949 (2016).
67. Brutsaert, W. *Evaporation into the Atmosphere: Theory, History, and Applications* (Springer, 1982).
68. Savitzky, A. & Golay, M. J. E. Smoothing and differentiation of data by simplified least squares procedures. *Anal. Chem.* **36**, 1627–1639 (1964).
69. Chen, J. et al. A simple method for reconstructing a high-quality NDVI time-series data set based on the Savitzky–Golay filter. *Remote Sens. Environ.* **91**, 332–344 (2004).
70. Deng, S., Tan, X., Liu, B., Yang, F. & Yan, T. A reversal in global occurrences of flash drought around 2000 identified by rapid changes in the standardized evaporative stress ratio. *Sci. Total Environ.* **848**, 157427 (2022).
71. Gong, Z. et al. The features of regional flash droughts in four typical areas over China and the possible mechanisms. *Sci. Total Environ.* **827**, 154217 (2022).
72. Gou, Q. et al. Application of an improved spatio-temporal identification method of flash droughts. *J. Hydrol.* **604**, 127224 (2022).
73. Hu, C. et al. A new framework for the identification of flash drought: multivariable and probabilistic statistic perspectives: identification of flash drought. *Int. J. Climatol.* **41**, 5862–5878 (2021).
74. Edris, S. G. et al. Analysis of the critical components of flash drought using the standardized evaporative stress ratio. *Agric. Forest Meteorol.* **330**, 109288 (2023).
75. Lisonbee, J., Woloszyn, M. & Skumanich, M. Making sense of flash drought: definitions, indicators, and where we go from here. *J. Appl. Serv. Climatol.* **2021**, 1–19 (2021).
76. Anderson, M. C., Norman, J. M., Mecikalski, J. R., Otkin, J. A. & Kustas, W. P. A climatological study of evapotranspiration and moisture stress across the continental United States based on thermal remote sensing: 1. Model formulation. *J. Geophys. Res. Atmos.* <https://doi.org/10.1029/2006JD007506> (2007).
77. Otkin, J. A. et al. Examining rapid onset drought development using the thermal infrared–based evaporative stress index. *J. Hydrometeorol.* **14**, 1057–1074 (2013).
78. Otkin, J. A., Anderson, M. C., Hain, C. & Svoboda, M. Examining the relationship between drought development and rapid changes in the evaporative stress index. *J. Hydrometeorol.* **15**, 938–956 (2014).
79. White, R. H. & Toumi, R. The limitations of bias correcting regional climate model inputs: bias correction limitations. *Geophys. Res. Lett.* **40**, 2907–2912 (2013).
80. Chen, J., Brissette, F. P. & Caya, D. Remaining error sources in bias-corrected climate model outputs. *Clim. Chang.* **162**, 563–582 (2020).
81. Maraun, D. Bias correcting climate change simulations - a critical review. *Curr. Clim. Chang. Rep.* **2**, 211–220 (2016).
82. Maraun, D. et al. Towards process-informed bias correction of climate change simulations. *Nat. Clim. Chang.* **7**, 764–773 (2017).

## Acknowledgements

This work was funded by the National Science Foundation grant OIA-1946093.

## Author contributions

J.I.C. conceived of the presented idea. J.I.C., E.R.M., J.B.B., and J.C.F. organized the outline and developed the methodology. J.A.O. developed the methodology. J.I.C. took the lead in writing the manuscript and provided figures. J.I.C., E.R.M., J.B.B., J.C.F., J.A.O., L.E.L.L., E.D.H., V.M., and X.X. contributed to the writing of the article.

## Competing interests

The authors declare no competing interests.

## Additional information

**Supplementary information** The online version contains supplementary material available at <https://doi.org/10.1038/s43247-023-00826-1>.

**Correspondence** and requests for materials should be addressed to Jordan I. Christian.

**Peer review information** *Communications Earth & Environment* thanks the anonymous reviewers for their contribution to the peer review of this work. Primary handling editors: Leiyl Chen, Heike Langenberg. Peer reviewer reports are available.

**Reprints and permission information** is available at <http://www.nature.com/reprints>

**Publisher's note** Springer Nature remains neutral with regard to jurisdictional claims in published maps and institutional affiliations.



**Open Access** This article is licensed under a Creative Commons

Attribution 4.0 International License, which permits use, sharing, adaptation, distribution and reproduction in any medium or format, as long as you give appropriate credit to the original author(s) and the source, provide a link to the Creative Commons license, and indicate if changes were made. The images or other third party material in this article are included in the article's Creative Commons license, unless indicated otherwise in a credit line to the material. If material is not included in the article's Creative Commons license and your intended use is not permitted by statutory regulation or exceeds the permitted use, you will need to obtain permission directly from the copyright holder. To view a copy of this license, visit <http://creativecommons.org/licenses/by/4.0/>.

© The Author(s) 2023